



Published in final edited form as:

J Dev Orig Health Dis. 2011 December ; 2(6): 322–329. doi:10.1017/S2040174411000572.

Analyzing growth trajectories

Ian W. McKeague¹, Sara López-Pintado², Marc Hallin³, and Miroslav Šiman⁴

^{1,2}Department of Biostatistics, Columbia University, 722 West 168th Street, 6th Floor, New York, NY 10032

³ECARES, Université libre de Bruxelles, 50 Avenue F. D. Roosevelt, 1050 Bruxelles, Belgium; ORFE, Princeton University; CentER, Tilburg University; ECORE; Académie Royale de Belgique

⁴Institute of Information Theory and Automation of the ASCR, Pod Vodárenskou věží 4, CZ-18208, Prague 8, Czech Republic

Abstract

Growth trajectories play a central role in life course epidemiology, often providing fundamental indicators of prenatal or childhood development, as well as an array of potential determinants of adult health outcomes. Statistical methods for the analysis of growth trajectories have been widely studied, but many challenging problems remain. Repeated measurements of length, weight and head circumference, for example, may be available on most subjects in a study, but usually only *sparse* temporal sampling of such variables is feasible. It can thus be challenging to gain a detailed understanding of growth patterns, and smoothing techniques are inevitably needed. Moreover, the problem is exacerbated by the presence of large fluctuations in growth velocity during early infancy, and high variability between subjects. Existing approaches, however, can be inflexible due to a reliance on parametric models, require computationally intensive methods that are unsuitable for exploratory analyses, or are only capable of examining each variable separately. This article proposes some new nonparametric approaches to analyzing sparse data on growth trajectories, with flexibility and ease of implementation being key features. The methods are illustrated using data on participants in the Collaborative Perinatal Project.

Keywords

Growth curves; nonparametric Bayes; data depth contours

1 Introduction

There is a vast literature on the statistical analysis of human growth curves. The earliest work in this area concentrated on the formulation of parametric growth models, with Jenss, Bayley, Preece, Baines, Count and Gompertz being prominent contributors. These models are designed to capture known features of growth and development (such as the mid-childhood growth spurt) and have reached a high degree of sophistication with broad applications^{1,2}. For example, such models have been used in searches for quantitative trait loci that control the key features of human growth trajectories³.

The purpose of the present article is to propose various new nonparametric modeling approaches that can bring greater flexibility, as well as ease of implementation, to the analysis of growth trajectories based on sparse data. Our emphasis is on methods that are suited for the study of prenatal or early childhood development, in which large fluctuations

Statement of Interest: None declared.

in growth velocity and high variability between subjects are not easily handled by parametric models. Despite a resurgent interest in the analysis of human growth trajectories, current statistical methods are limited by an over-reliance on parametric modeling and are only capable of examining each variable separately, or require computationally intensive methods that are unsuitable for exploratory analyses. Repeated measurements of length, weight, BMI and head circumference, for example, may be available on most subjects in a study, but usually only *sparse* temporal sampling of such variables is feasible. It can thus be challenging to gain a detailed understanding of growth patterns, and smoothing techniques are inevitably needed. Moreover, the problem is exacerbated by the presence of large fluctuations in growth velocity during early infancy, and high variability between subjects.

We propose a nonparametric Bayesian method⁴ for reconstructing growth velocity curves from sparse temporal data (or repeated measures) on a single variable. Figure 1 illustrates this method as applied to length measurements in a sample of 532 girls who participated in the Collaborative Perinatal Project (see Section 4 for further details). The left panel shows the reconstructed growth velocity curve (along with error bounds) of a specific individual, and the right panel replicates this for the whole sample. A key advantage of this method over existing approaches is that error bounds are included in the reconstruction. A version of data depth that is suitable for visualizing *functional* data⁵ is also discussed; the right panel of Fig. 1 highlights the deepest growth velocity curve in the sample and can be interpreted as a functional equivalent of the sample median.

In addition, we propose a method for visualizing patterns in the growth trajectories of *multiple* variables. Commonly used growth charts produce plots of univariate quantile curves, but such plots clearly omit all information related to dependencies between the various measurements under study. This is potentially misleading, as growth charts are often used as a diagnostic tool for detecting possible outliers, while a multivariate outlier clearly need not be an outlier from a marginal point of view, and vice versa. To address this problem, we introduce a method based on Tukey's notion of halfspace data depth⁶, leading to the construction of flexible multiple-output growth charts, see for example Fig. 5.

2 Growth velocities

Nonparametric frequentist approaches to the analysis of growth trajectories have been extensively studied in the setting of functional data analysis^{7,8}. In particular, functional principal components analysis is used when it is of interest to estimate the “dominant modes of variation” of a sample of trajectories. Typically, however, a crucial first step is needed before such analyses are possible: the trajectories need to be reconstructed on a fine grid of equally spaced time points. Methods for reconstructing trajectories in this way have been studied using kernel smoothing⁷, smoothing splines⁸, local linear smoothing⁹, mixed effects models^{10,11}, and principal components analysis through conditional expectations^{12,13}.

In many settings involving functional data, the *gradients* of the trajectories (i.e., growth velocities) are of central interest, rather than the trajectories themselves, especially when dynamical effects are concerned. Difference quotients between observation times can be used to generate simple approximate gradients, but these estimates are piecewise constant and would not be suitable for use in functional data analysis unless the observation times are dense. In the case of regularly spaced observation times, spline smoothing to approximate the gradient of the trajectory over a fine grid is recommended⁸. More generally, methods of numerical differentiation, including spline smoothing, are an integral part of the extensive literature on ill-posed inverse problems for linear operator equations. In this literature, the observation times are usually viewed as becoming dense (for the purpose of showing

convergence)¹⁴; in particular, the assumption of asymptotically dense observation times plays a key role in the study of penalized least squares estimation and cross-validation^{15,16}.

Growth velocities can be reconstructed given sparse and irregularly spaced observation times (one observation time per trajectory is even enough) by borrowing strength between the trajectories in the data set. For such sparse observations, it has been shown that the best linear predictor of the gradient can be estimated in terms of estimated principal component scores, assuming Gaussian trajectories and that the pooled observation times become dense¹⁷. A disadvantage of this approach, however, is that data at the individual level plays a relatively minor role in the reconstruction, and its accuracy depends on how well each individual gradient can be represented in terms of a small number of estimated principal component functions (this in turn would require an accurate estimate of the covariance kernel of the trajectories, an unlikely scenario in the case of sparse observation times).

López-Pintado and McKeague (2011)^{4,18} recently developed a flexible Bayesian approach to reconstructing growth velocities from sparse data, as outlined in the next section. Their approach is designed to adapt to observation times that are both sparse and irregularly spaced, and that can vary across subjects. The observation times are allowed to be arbitrary, as long as they include the endpoints of the time interval (so interpolation is possible). The prior distribution for the growth velocity is specified by a multivariate normal distribution at the observation times, and a tied-down Brownian motion between the observation times. This leads to an explicit representation of the posterior distribution in a way that *exactly reproduces* the data at the observation times. The empirical Bayes approach is then used to estimate the hyperparameters in the prior, borrowing strength between subjects, but in a simpler fashion than estimating principal component scores¹⁷. An important aspect of this approach is that reconstructed gradients can be computed rapidly over a fine grid, and then used directly as input into existing software, without the need for sophisticated smoothing techniques. Furthermore, a comparison of the results from repeated draws from the posterior distribution (multiple imputation) provides an easy way of assessing uncertainty in the conclusions (of standard functional data analyses) due to data sparsity.

The empirical Bayes approach is well developed for reconstructing individual growth velocity curves from *parametric* growth models¹⁹. A nonparametric Bayesian growth curve model has been developed for testing for differences in growth patterns between groups of individuals²⁰. In addition, a nonparametric hierarchical-Bayesian growth curve model for reconstructing individual growth curves is available, but requires the use of computationally intensive Markov chain Monte Carlo methods²¹.

Bayesian reconstruction

We first consider how to reconstruct a growth velocity curve for a single subject. The observation times will typically vary slightly across the sample, but will be clustered around certain *nominal* ages (e.g., birth, 4 months, 8 months, 1 year, ...). Let the observation times for the specific individual be $0 = t_1 < t_2 < \dots < t_p = T$, and assume that the endpoints of the time interval over which the reconstruction is needed are included. Letting the subject's growth velocity at age t be $X(t)$, the statistical problem is to estimate the growth velocity curve $X = \{X(t), 0 \leq t \leq T\}$ from data on its integral over the gaps between the observation times. Reconstructing X based on such data is an ill-posed inverse problem in the sense that no unique solution exists, so some type of external information or constraint (i.e., *regularization*) is needed to produce a unique solution¹⁴.

The difference quotient estimate of $X(t)$ in the interval between the i th and $(i+1)$ th observation times is given by

$$y_i = \frac{1}{\Delta_i} \int_{t_i}^{t_{i+1}} X(s) ds,$$

where Δ_j is the length of the interval. Higher order difference estimates are produced by taking into account the proximity to neighboring observation times, say replacing y_i by the weighted estimate $\bar{y}_i = w_i y_{i-1} + (1 - w_i) y_i$, where $w_i = \Delta_i / (\Delta_{i-1} + \Delta_i)$ for $i = 2, \dots, p - 1$. Neither of these estimates borrow strength from other trajectories in the sample, but they provide the building blocks of empirical Bayes estimators that take advantage of the whole sample, as we now explain.

In the Bayesian approach to ill-posed inverse problems, regularization takes the form of specifying a prior distribution on X . It is desirable to make the prior flexible enough to cover a broad range of growth velocity patterns, yet simple enough that it is tractable to find the posterior distribution without the need for computationally intensive methods. López-Pintado and McKeague (2011)⁴ showed that this can be done using the following hierarchical prior: 1) at the observation times, $\mathbf{X} = (X(t_1), \dots, X(t_p))'$ has a p -dimensional normal distribution with mean $\boldsymbol{\mu}_0$ and non-singular covariance matrix $\boldsymbol{\Sigma}_0$, and 2) the conditional distribution of X given \mathbf{X} is a tied-down Brownian motion with given infinitesimal variance $\sigma^2 > 0$. Allowing an arbitrary (multivariate normal) prior at the observation times provides flexibility that would not be possible using a Brownian motion prior for the whole of X . In addition, the availability of data at these time points makes it possible to specify the hyperparameters in the multivariate normal (as we discuss below), which is crucial for practical implementation of our approach.

The posterior mean of X takes the computationally tractable form of a quadratic spline with knots at the observation times:

$$\widehat{\mu}(t) = \widehat{\mu}_i + [\widehat{\mu}_{i+1} - \widehat{\mu}_i](t - t_i) / \Delta_i + 6(t - t_i)(t_{i+1} - t) [y_i - (\widehat{\mu}_i + \widehat{\mu}_{i+1}) / 2] / \Delta_i^2$$

for t belonging to the interval between the i th and $(i + 1)$ th observation times. Integration shows that $\widehat{\mu}(t)$ exactly reproduces the data. Here $\widehat{\mu}_i$ is the i th component of the posterior mean of \mathbf{X} , given by $\widehat{\boldsymbol{\mu}} = (\sum_0^{-1} + \mathbf{Q})^{-1} (\sum_0^{-1} \boldsymbol{\mu}_0 + \mathbf{D}\mathbf{Y})$ where $\mathbf{Y} = (y_1, \bar{y}_2, \dots, \bar{y}_{p-1}, y_p)'$,

$$\mathbf{Q} = \frac{3}{\sigma^2} \begin{pmatrix} \frac{1}{\Delta_1} & \frac{1}{\Delta_1} & 0 & \dots & 0 \\ \frac{1}{\Delta_1} & \frac{1}{\Delta_1} + \frac{1}{\Delta_2} & \frac{1}{\Delta_2} & \ddots & \vdots \\ 0 & \frac{1}{\Delta_2} & \ddots & \ddots & 0 \\ \vdots & \ddots & \ddots & \ddots & \frac{1}{\Delta_{p-1}} \\ 0 & \dots & 0 & \frac{1}{\Delta_{p-1}} & \frac{1}{\Delta_{p-1}} \end{pmatrix},$$

and

$$\mathbf{D} = \frac{6}{\sigma^2} \text{diag} \left(\frac{1}{\Delta_1}, \dots, \frac{1}{\Delta_{i-1}} + \frac{1}{\Delta_i}, \dots, \frac{1}{\Delta_{p-1}} \right).$$

The posterior distribution is Gaussian, with a covariance kernel (not depending on \mathbf{Y}) that takes a similarly tractable form as the mean.

The posterior mean $\hat{\mu}(t)$ can be used for reconstructing the unobserved growth velocity $X(t)$, provided various hyperparameters are specified in advance: the prior mean μ_0 and prior precision matrix Σ_0^{-1} . This is done via a nonparametric empirical Bayes approach applied to the full sample of trajectories, initially treated as having *identical* sets of (nominal) observation times. The sample mean of \mathbf{Y} is used to specify μ_0 . A constrained l_1 minimization method of sparse precision matrix estimation (clime)²² is applied to the (singular) sample covariance matrix of \mathbf{Y} to specify Σ_0^{-1} . By restricting the resulting posterior covariance kernel and mean to the *actual* observation times for a given subject, we obtain suitable hyperparameters across the whole sample that adjust for any changes from the nominal observation times⁴.

The infinitesimal standard deviation σ is a smoothing parameter (playing the role of a time-scale), and can be selected using a type of cross-validation based on the prediction error from leaving-out an interior observation time⁴. We have found that $\hat{\mu}(t)$ is relatively insensitive to σ . On the other hand, the width of credible intervals around $\hat{\mu}(t)$ is roughly proportional to σ . In practice, insight into an appropriate choice of σ can also be gained through inspecting plots of $\hat{\mu}(t)$, say for values σ in the range 1–3 for the height data (as suggested by cross-validation), and it is worthwhile to include pointwise 95% credible intervals around $\mu\sigma(t)$ as a way of assessing the uncertainty in the reconstruction (see Fig. 3 for examples).

An R package “growthrate” implementing this reconstruction method has been developed by López-Pintado and McKeague (2011)¹⁸. The package includes the data set and examples of the code used to compute the reconstructed growth velocity curves displayed in this article, and is available on the CRAN archive²³.

Functional data depth

Given a sample of reconstructed growth velocity curves, it is of interest to look for “outlying” patterns of growth. One way to do this is to use the notion of functional data depth recently developed by López-Pintado and Romo (2009)⁵ with the aim of introducing robust methods into functional data analysis. Robust methods are even more relevant in a functional setting than in multivariate problems because outliers can affect functional statistics in more ways and they can be more difficult to detect. For instance, a curve could be an “outlier” without having any unusually large value. This notion of depth is particularly convenient for identifying outliers because shape is also relevant in addition to magnitude. Direct generalization of multivariate depth (discussed in the next section) to functional data often leads to either depths that are computationally intractable or depths that do not take into account some natural properties of the functions, such as shape.

Let $x_1(t), \dots, x_n(t)$ be a sample of real-valued functions defined on the time interval $[0, T]$. The *band* delimited by these curves is the set of points (t, y) such that $x_i(t) < y < x_j(t)$ for some $i, j = 1, \dots, n$. An example for the case of $n = 3$ curves is provided in Figure 2. The *band depth* of a function $x(t)$ is then defined as $D_{n,J}(x) = p_1 + \dots + p_J$, where $J \geq 2$ is fixed, and p_j is the proportion of bands that contain the graph of x among the bands derived from j curves in the sample. In the sequel we use band depth with $J = 3$, which is recommended⁵ for several reasons: 1) when J is larger than 3 the index $D_{n,J}$ can be computationally intensive, 2) bands corresponding to large values of J do not resemble the shape of *any* of the curves from the sample, 3) the band depth induced order is very stable in J , and 4) the

band depth with $J=2$ is the easiest to compute, but if two curves cross, the band delimited by them is degenerate at a point and it is unlikely that any other curve will be inside this band.

3 Growth charts and statistical depth

In this section we discuss the use of statistical depth for analyzing *multiple* growth variables (e.g., head circumference, weight and height) at fixed ages (in contrast to single variables at multiple ages, as studied in the previous section). Statistical depth was first considered for multivariate data to generalize order statistics, ranks and medians to higher dimensions. Given a probability distribution P on k -dimensional Euclidean space, the depth of a k -vector \mathbf{x} represents the probability that a random draw from P is “more of an outlier” than \mathbf{x} . Various definitions of multivariate depth have been proposed and analyzed^{24,25,26,27,28,29}. The notion has been applied, for instance, as an attempt to extend rank tests to a multivariate context³⁰, in control charts for multivariate processes³¹, confidence regions³², regression³³, and for visualizing sample dispersion³⁴.

Our discussion of multiple output growth charts involves Tukey’s notion of *halfspace* depth²⁵, which is defined as follows. Consider all hyperplanes running through \mathbf{x} : each Π divides \mathbb{R}^k into two closed halfspaces, with probabilities P_{Π}^+ and P_{Π}^- , respectively. Putting $P_{\Pi} = \min(P_{\Pi}^-, P_{\Pi}^+)$, select the hyperplane Π^* , say, for which that probability P_{Π} reaches a minimum: that minimum is called the halfspace depth $d_P(\mathbf{x}) = P_{\Pi^*} = \min_{\Pi} P_{\Pi}$ of \mathbf{x} with respect to P .

The collection of all points \mathbf{x} with given halfspace depth $d_P(\mathbf{x})$ is called a *depth contour*. An empirical version of this definition leads to the construction of *empirical depth contours*. Just as their population counterparts, empirical depth contours have the attractive geometric property that they enclose nested, convex sets. Besides, empirical depth contours are polytopes, each face of which runs through exactly k sample points (when generated from a continuous distribution P). For $k=1$, depth contours reduce to pairs of quantiles of complementary order, τ and $1-\tau$, where $0 < \tau < 1$.

Quantile contours

The collection of empirical depth contours provides an interesting picture of the sample at hand, and a powerful data-analytical tool. Unfortunately, however, effective computation of depth contours was based, until recently, on algorithms with prohibitive complexity as k grows, and hardly implementable beyond $k=2$ or 3 (although approximate methods are available^{35,36,37}).

Hallin, Paindaveine and Šiman (2010)³⁸ recently established a strong connection between half-space depth and regression quantiles. That connection has two important benefits: a quantile-based interpretation of depth contours, and, perhaps even more importantly, bringing the power of linear programming techniques to the practical computation of empirical contours. Moreover, that connection also opens the way to a tractable definition of (multiple-output) regression depth, and depth-based multiple-output growth charts.

First recall that the classical quantile of order τ , in a univariate sample X_1, \dots, X_n , can be defined as a minimizer of $\sum_{i=1}^n \rho_{\tau}(X_i - a)$ over $a \in \mathbb{R}$, where $\rho_{\tau}(x) = x(\tau - I[x < 0])$ is the check function, and I is the indicator function; in the case $\tau = 1/2$, note that $\rho_{\tau}(x) = |x|/2$. This definition of quantiles naturally extends to a k -dimensional sample $\mathbf{X}_1, \dots, \mathbf{X}_n$, with the *empirical quantile hyperplane of order τ* defined as a hyperplane $\Pi_{\tau} = \{\mathbf{x}: x_k = \mathbf{b}'_{\tau}(x_1, \dots, x_{k-1}) + a_{\tau}\}$ that minimizes, over $(a, \mathbf{b}') \in \mathbb{R}^k$, the sum

$$\sum_{i=1}^n \rho_{\tau}(X_{i,k} - a - \mathbf{b}'(X_{i,1}, \dots, X_{i,k-1})')$$

of *vertical* weighted deviations, with the k th component representing the vertical direction. Now, choose an arbitrary unit vector $\mathbf{u} \in S_{k-1}$, the unit sphere in \mathbb{R}^k , and consider it as the “vertical” direction: the “vertical” component of a vector \mathbf{X} is then $(\mathbf{u}'\mathbf{X})\mathbf{u}$ and, denoting by $\Gamma_{\mathbf{u}}$ a $k \times (k-1)$ matrix of column unit vectors such that $(\mathbf{u}, \Gamma_{\mathbf{u}})$ constitutes an orthonormal basis of \mathbb{R}^k , we have $\mathbf{X} = \mathbf{u}(\mathbf{u}'\mathbf{X}) + \Gamma_{\mathbf{u}}(\Gamma_{\mathbf{u}}'\mathbf{X})$. Letting $\boldsymbol{\tau} = \boldsymbol{\tau}\mathbf{u}$, the *directional empirical quantile hyperplane of order τ for direction \mathbf{u}* is obtained as in the above display, but with \mathbf{u} characterizing the vertical direction, yielding a hyperplane $\Pi_{\boldsymbol{\tau}} = \{\mathbf{x} : \mathbf{u}'\mathbf{x} = \mathbf{b}'\Gamma_{\mathbf{u}}'\mathbf{x} + a_{\boldsymbol{\tau}}\}$ minimizing, over $(a, \mathbf{b}') \in \mathbb{R}^k$, the sum

$$\sum_{i=1}^n \rho_{\tau}(\mathbf{u}'\mathbf{X}_i - a - \mathbf{b}'(\Gamma_{\mathbf{u}}'\mathbf{X}_i))$$

of weighted deviations along direction \mathbf{u} , with weights $(1 - \tau)$ or τ according as \mathbf{X}_i lies above or below the hyperplane. Fixed- τ collections of $\Pi_{\boldsymbol{\tau}}$ hyperplanes define polyhedral *empirical quantile contours* of order τ by means of the intersections of upper halfspaces corresponding to all the quantile hyperplanes of the same quantile level τ . Population versions are obtained in the same way, with sums replaced by mathematical expectations.

Quantile contours can be easily computed by parametric linear programming methods that can handle even samples up to size 500 and dimension $k = 5$; see Paindaveine and Šiman (2011)³⁹. The main finding in Hallin, Paindaveine and Šiman (2010)³⁸ is that halfspace depth contours and quantile contours actually coincide. As a consequence, quantile contours inherit the geometric features of depth contours mentioned earlier, benefit from the interpretation and the analytical features of quantiles, and allow linear programming numerical implementation. Another benefit is the possibility of reconstructing conditional depth/quantile contours via local methods—providing a convincing definition of (multiple output) regression depth contours and paving the way for the construction of multiple output growth charts, as explained in the next section.

Multiple output growth charts

Growth charts are expected to describe the distributions of selected body measurements in children, as a function of age. That description takes the form of a plot of quantiles against age. Existing methods are usually limited to producing *marginal* growth charts, that is, plots of univariate quantile curves. Such plots clearly omit all information related with dependencies between the various measurements under study. This is regrettable, as growth charts are often used as a diagnostic tool for detecting possible outliers, while a multivariate outlier clearly need not be an outlier from a marginal point of view, and vice versa. A semiparametric approach to multiple-output growth charts has been studied by Wei (2008)⁴⁰.

The local methods described in a preprint of Hallin, Lu, Paindaveine and Šiman (2011)⁶ allow for nonparametric multiple-output growth charts, hence a joint inspection of several measurements as a function of age. Let (t_i, \mathbf{X}_i) , $i = 1, \dots, n$, be a random sample of k -dimensional growth measurements \mathbf{X}_i , along with the age t_i at which each observation was made. We are interested in using these data to infer the depth/quantile contours of \mathbf{X} at a

given age t_0 (which may not be among the observation times). The local constant method consists in computing the weighted depth/quantile hyperplanes $\Pi_{\tau}^{t_0} = \{\mathbf{x} | \mathbf{u}' \mathbf{x} = \mathbf{b}'_{\tau} + \Gamma'_{\mathbf{u}} \mathbf{x} + a_{\tau}^{t_0}\}$ minimizing, over $(a, \mathbf{b}') \in \mathbb{R}^k$, the sum

$$\sum_{i=1}^n w_i(t_0) \rho_{\tau}(\mathbf{u}' \mathbf{X}_i - a - \mathbf{b}' (\Gamma'_{\mathbf{u}} \mathbf{X}_i))$$

with \mathbf{u} ranging over the unit sphere S_{k-1} ; the weights are of the type considered in traditional kernel methods: $w_i(t_0) = K((t_i - t_0)/h)/h$ for some univariate density K and bandwidth $h > 0$. For any given t_0 , this method yields a collection of nested “horizontal” cylinders (with respect to the t -axis), the intersection of which with the hyperplane $t = t_0$ provides a reconstruction of the depth/quantile contours of \mathbf{X} at age t_0 ; such an intersection is called a t_0 -cut (see Fig. 5 for examples). These cuts can be obtained exactly by means of the algorithm and Matlab code presented in Paidaveine and Šiman (2011)³⁹.

4 Application to CPP data

In this section, we present some examples to illustrate the methods we have introduced. All the examples use data collected from participants in the Collaborative Perinatal Project (CPP) from examinations at the (nominal) ages of birth, four, eight, and twelve months, and three, four, and seven years. Here, by the “nominal” age we mean the targeted age of the measurement; the actual age of the measurement varies around the nominal age.

Example 1: Growth velocity curves

In our first example, we use the following inclusion criteria: female, birthweight 1800–4000 gms, gestational age 37–42 weeks, non-breast-fed, maternal age 20–40 years, the mother did not smoke during pregnancy, complete data on length and actual examination age, and increasing length measurements with age of examination (about 1% of the subjects were excluded under this criterion). This results in a data set of $p = 7$ height measurements on each of $n = 532$ subjects. As mentioned in Section 2, this data set is provided in the R package `growthrate`¹⁸, which also includes the code used to produce the growth velocity curves displayed below.

Figure 3 gives the reconstructed growth velocity curves (of length) for two subjects, and for three choices of σ . The choice $\sigma = 1$ produces very tight bands, which may be unrealistic because the growth rate is unlikely to have sharp bends at the observation times; the more conservative choices $\sigma = 2$ and 3 allow enough flexibility in this regard and appear to be more reasonable. Notice that the $\sigma = 2$ and $\sigma = 3$ bands bulge between observation times (and this is especially noticeable in the last observation time interval), which is a desirable feature since we would expect greater precision in the estimates close to the observation times.

Figure 4 is based on the notion of band depth defined at the end of Section 2, which allows the ordering of a sample of curves from the center outwards and consequently to define the middle 50% of curves, generalizing the notion of the classical boxplot to functional data. An R package “`fbplot`” for computing functional boxplots has been developed by Sun and Genton (2011)⁴¹. Such plots provide a useful diagnostic tool for detecting unusual patterns in the *shape* of individual growth velocity curves. In addition, the information provided by data depth could be used to create a variable describing the extent to which a subject has an unusual growth pattern, and used for predicting adult health outcomes. For example,

regressing IQ at age seven on the indicator “not in the deepest 50%” and adjusting for various other covariates (birthweight, birthlength and gestational age), suggests that an unusual growth pattern is (negatively) associated with IQ (data not shown).

Example 2: Bivariate growth charts

This example is based on CPP data for 1775 girls from the Boston site, restricted to subjects having complete data on length, weight and head circumference. The monotonicity of length and head circumference as functions of age was violated (by more than 4 cm for length, and 3 cm for head circumference) by 12 individuals; those 12 highly suspicious observations were excluded, which still left $n = 1268$ complete records for the analysis.

Figure 5 displays the multiple output growth charts described earlier. The two plots show the bivariate t_0 -cuts of the growth trajectories of weight (kgs) and head circumference (cms), and length (cms) and head circumference (cms), at five equispaced ages between birth and 7 years. Head circumference is on the vertical axis in each plot. Clearly there is a much higher correlation between the pairs of variables at earlier ages than at later ages, especially in the left panel. These plots provide a useful diagnostic tool for detecting unusual patterns of growth in *combinations* of variables, and that might not be noticed in standard growth charts that examine each variable separately. For example, these pictures illustrate age dependence of both the correlation structure and the ratios of the plotted characteristics that could not be detected from the marginal univariate growth charts. The two plots also clearly show that marginal outliers need not be multivariate outliers and vice versa. Consequently, bivariate growth charts would rightly diagnose some children with small head circumference and small length or weight as normal even when the univariate growth charts indicated the contrary. Needless to say, depth contours could be constructed for any age, e.g., for the reference ages or for the age of a child under particular investigation.

5 Conclusion

We have proposed various new nonparametric methods for the analysis of growth trajectories, bringing greater flexibility as well as ease of implementation to existing approaches. For the CPP data set, these methods can lead to interesting findings about early childhood growth patterns. First we reconstructed growth velocity curves using an empirical Bayes technique that adapts to data sparsity and gives a way of assessing uncertainty in the reconstruction. Second, we discussed the use of functional data depth and functional boxplots which provide useful diagnostic tools for detecting unusual patterns in growth trajectories. Finally, using regression quantiles and Tukey’s notion of data depth, we proposed flexible and robust growth charts for multiple variables.

Acknowledgments

The research of Ian McKeague was supported in part by NIH grant R01 GM095722 (PI: McKeague) and NIH grant P01 AG 023028-01; he also gratefully acknowledges the help and encouragement of Ezra Susser. The research of Sara López-Pintado was supported by Spanish Ministry of Education and Science grant SEJ2007-67734. The research of Marc Hallin was supported by Sonderforschungsbereich “Statistical modelling of nonlinear dynamic processes” (SFB 823) of the Deutsche Forschungsgemeinschaft, and by a Discovery Grant of the Australian Research Council. The research of Miroslav Šiman was supported by Project 1M06047 of the Ministry of Education, Youth and Sports of the Czech Republic.

References

1. Dasgupta, P.; Hauspie, R. Perspectives in Human Growth, Development and Maturation. Kluwer Academic Publishers; 2001.

2. Sumiya T, Tashima T, Nakahara H, Shohoji T. Relationships between biological parameters of Japanese growth of height. *Environmetrics*. 2001; 12:367–382.
3. Li N, Das K, Wu R. Functional mapping of human growth trajectories. *Journal of Theoretical Biology*. 2009; 261(1):33–42. [PubMed: 19632241]
4. López-Pintado S, McKeague IW. Recovering gradients from sparsely observed functional data. *Biometrics*. 2011. under revision.
<http://www.columbia.edu/~im2131/ps/growthrate-package-reference.pdf>
5. López-Pintado S, Romo J. On the concept of depth for functional data. *Journal of the American Statistical Association*. 2009; 104(486):718–734.
6. Hallin M, Lu Z, Paindaveine D, Šiman M. Local bilinear multiple-output quantile regression and regression depth. 2011 Preprint.
7. Ferraty F, Vieu P. *Nonparametric Functional Data Analysis*. Springer; New York: 2006.
8. Ramsay JO, Silverman BW. *Functional Data Analysis*. Springer; New York: 2005.
9. Hall P, Müller HG, Wang JL. Properties of principal components methods for functional and longitudinal data analysis. *Annals of Statistics*. 2006; 34:1493–1517.
10. James G, Hastie TJ, Sugar CA. Principal component models for sparse functional data. *Biometrika*. 2000; 87:587–602.
11. Rice J, Wu C. Nonparametric mixed effects models for unequally sampled noisy curves. *Biometrics*. 2000; 57:253–259. [PubMed: 11252607]
12. Yao F, Müller HG, Wang JL. Functional data analysis for sparse longitudinal data. *Journal of the American Statistical Association*. 2005; 100:577–590.
13. Yao F, Müller HG, Wang JL. Functional linear regression analysis for longitudinal data. *Annals of Statistics*. 2005; 33:2873–2903.
14. Kirsch, A. *Applied Mathematical Sciences*. Springer-Verlag; New York: 1996. *An Introduction to the Mathematical Theory of Inverse Problems*, volume 120 of.
15. Nashed MZ, Wahba G. Convergence rates of approximate least squares solutions of linear integral and operator equations of the first kind. *Mathematics of Computation*. 1974; 28:69–80.
16. Wahba G. Practical approximate solutions to linear operator equations when the data are noisy. *SIAM Journal on Numerical Analysis*. 1977; 14(4):651–667.
17. Liu B, Müller HG. Estimating derivatives for samples of sparsely observed functions, with application to online auction dynamics. *Journal of the American Statistical Association*. 2009; 104:704–717.
18. López-Pintado S, McKeague IW. Growthrate: Bayesian reconstruction of growth velocity. R package version 1.0. 2011. <http://CRAN.R-project.org/package=growthrate>
19. Shohoji T, Kanefuji K, Sumiya T, Qin T. A prediction of individual growth of height according to an empirical Bayesian approach. *Annals of the Institute of Statistical Mathematics*. 1991; 43:607–619.
20. Barry D. A Bayesian model for growth curve analysis. *Biometrics*. 1995; 51(2):639–655. [PubMed: 7662851]
21. Arjas E, Liu L, Maglaperidze N. Prediction of growth: a hierarchical Bayesian approach. *Biometrical Journal*. 1997; 39:741–759.
22. Cai T, Liu W, Luo X. A constrained ℓ_1 minimization approach to sparse precision matrix estimation. *Journal of the American Statistical Association*. 2011; 106:594–607.
23. R Development Core Team. *R: A Language and Environment for Statistical Computing*. R Foundation for Statistical Computing; Vienna, Austria: 2011. <http://www.R-project.org/>
24. Mahalanobis PC. On the generalized distance in statistics. *Proceedings of the Natural Academy of Science of India*. 1936; 13:1305–1320.
25. Tukey JW. Mathematics and the picturing of data. *Proceedings of the International Congress of Mathematicians; Vancouver, B C*. 1974; 1975. p. 523-531. *Canad. Math. Congress, Montreal, Que*
26. Oja H. Descriptive statistics for multivariate distributions. *Statistics and Probability Letters*. 1983; 1:327–332.
27. Liu R. On a notion of data depth based on random simplices. *Annals of Statistics*. 1990; 18:405–414.

28. Fraiman R, Meloche J. Multivariate L-estimation. *Test*. 1999; 8:255–317.
29. Zuo Y, Serfling RJ. General notions of statistical depth function. *Annals of Statistics*. 2000; 28:461–482.
30. Liu R, Singh K. A quality index based on data depth and multivariate rank test. *Journal of the American Statistical Association*. 1993; 88:257–260.
31. Liu R. Control charts for multivariate processes. *Journal of the American Statistical Association*. 1995; 90:1380–1388.
32. Yeh A, Singh K. Balanced confidence sets based on Tukey depth. *Journal of the Royal Statistical Society Ser B*. 1997; 3:639–652.
33. Rousseeuw, P.; Leroy, AM. *Robust Regression and Outlier Detection*. Wiley; New York: 1987.
34. Liu R, Parelius JM, Singh K. Multivariate analysis by data depth: Descriptive statistics, graphics and inference. *Annals of Statistics*. 1999; 27:783–858.
35. Zuo Y. Multidimensional trimming based on projection depth. *Annals of Statistics*. 2006; 34(5): 2211–2251.
36. Cuesta-Albertos JA, Nieto-Reyes A. The random Tukey depth. *Computational Statistics and Data Analysis*. 2008; 52(11):4979–4988.
37. Kong L, Mizera I. Quantile tomography: using quantiles with multivariate data. 2010 Preprint, arXiv:0805.0056v1.
38. Hallin M, Paindaveine D, Šíman M. Multivariate quantiles and multiple-output regression quantiles: from L_1 optimization to halfspace depth. *Annals of Statistics*. 2010; 38(2):635–669.
39. Paindaveine D, Šíman M. Computing multiple-output regression quantile regions. *Computational Statistics and Data Analysis*. 2011 to appear.
40. Wei Y. An approach to multivariate covariate-dependent quantile contours with application to bivariate conditional growth charts. *Journal of the American Statistical Association*. 2008; 103(481):397–409.
41. Sun Y, Genton MG. Functional boxplots. *Journal of Computational and Graphical Statistics*. 2011; 20:316–334.

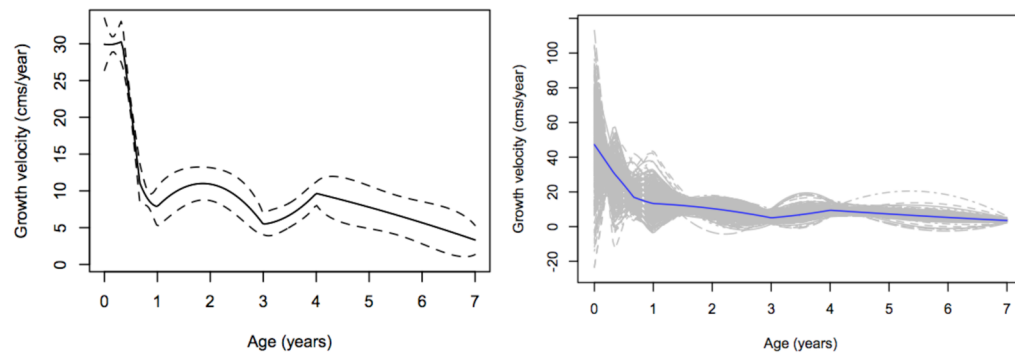


Figure 1.

The left panel shows the reconstruction of an individual growth velocity curve (solid line) with error bounds (dashed lines); the right panel shows the reconstructed growth velocity curves for all individuals in the sample with the deepest curve highlighted.

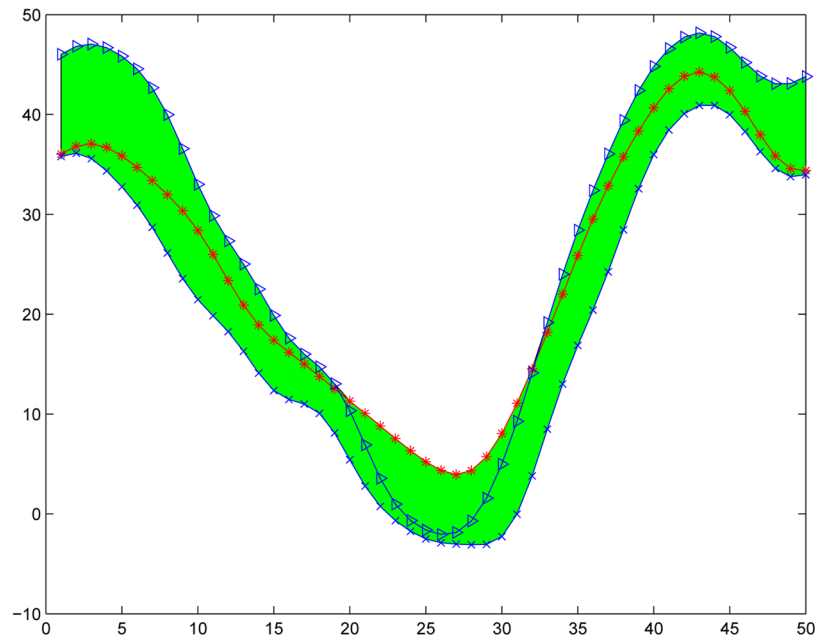


Figure 2.
A band determined by three curves (the shaded region), as used in the definition of functional data depth.

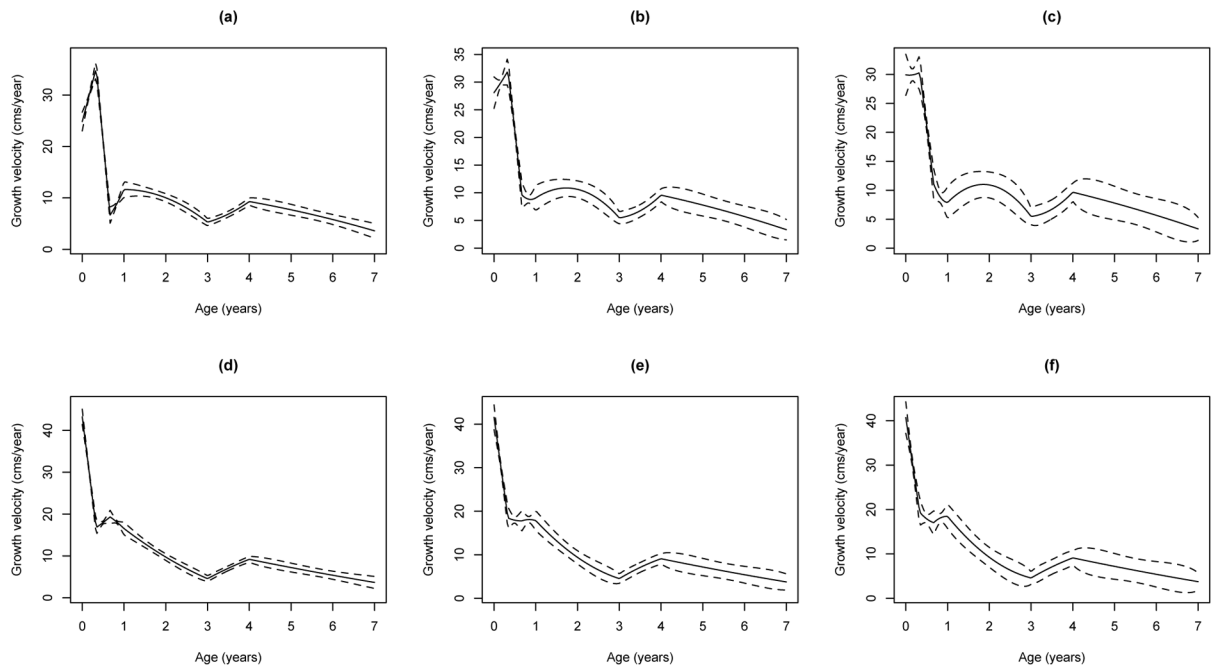


Figure 3. Reconstructed growth velocity curves for two subjects in Example 1; posterior mean $\hat{\mu}(t)$ (solid line), pointwise 95% credible intervals (dashed lines) based on $\sigma = 1, 2, 3$ in (a,d), (b,e) and (c,f), respectively; for one subject in (a,b,c), and a second subject in (d,e,f).

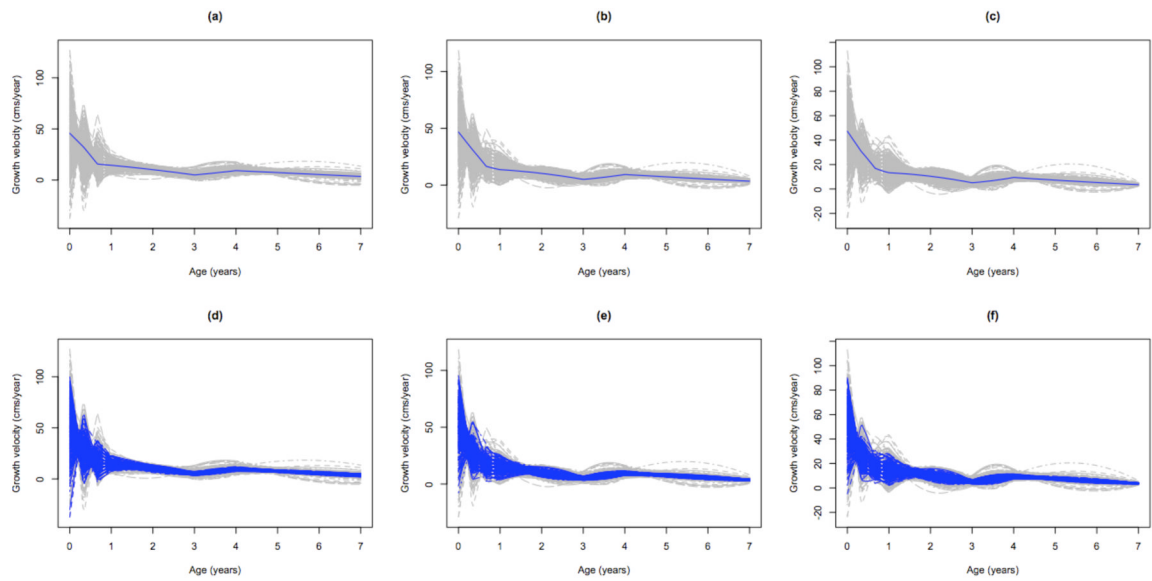


Figure 4. Reconstructed growth velocity curves for the whole sample in Example 1 based on $\sigma = 1, 2, 3$ in (a,d), (b,e) and (c,f), respectively; the dark line in (a,b,c) is the deepest curve, and the dark bands in (d,e,f) are functional boxplots (representing the deepest 50% of the curves).

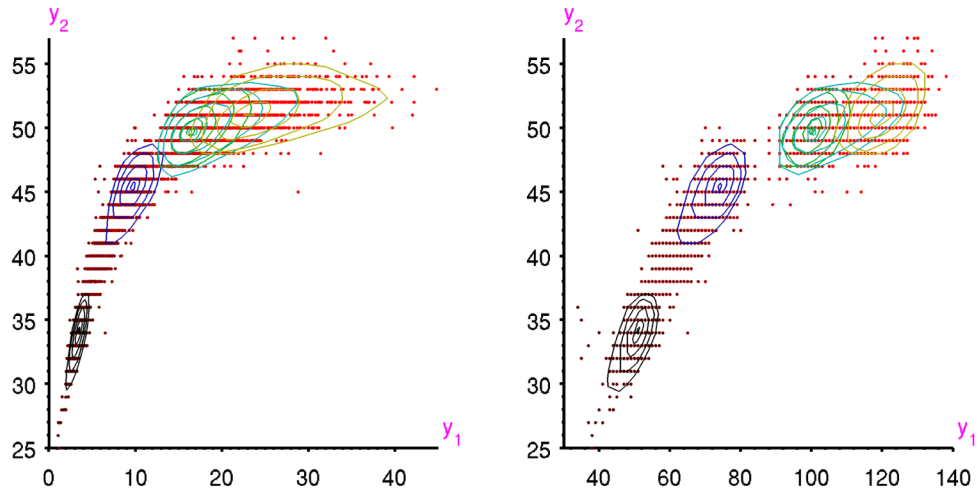


Figure 5. Estimated age-specific depth contours (cuts) in Example 2 for [left panel] head circumference (y_2) and weight (y_1), and [right panel] head circumference (y_2) and length (y_1), at equispaced ages $t_0 = 0$ (birth; black), 1.75 (blue), 3.5 (green), 5.25 (cyan) and 7 (yellow) years. Observations are shown by dots (darker for younger subjects, lighter for older ones).